Gmail

Geunhyeong Lee <ghlee1129@gmail.com>

Nuclear Science and Techniques - Decision on Manuscript ID NST-2025-0764.R2

1 개의 메일

Nuclear Science and Techniques <onbehalfof@manuscriptcentral.com> 2025년 12월 23일 AM 12:17
답장 주소: NST@sinap.ac.cn
받는사람: ghLee1129@gmail.com

23-Dec-2025

Dear Dr. Lee,

It is a pleasure to accept your manuscript entitled "Optimization of the FRIB Beam Dump: A Hybrid Genetic Algorithm and Reinforcement Learning Approach" for publication in Nuclear Science and Techniques.

You can monitor the progress of your article through the publication system by going to the web address www.springer.com/41365.

Normally, the pre-publication process takes up to a couple of months. During this period, galley proofs will be sent to you for checking and corrections purposes. The galley proofs must be returned to the production office within 2 calendar days.

Please note that Nuclear Science and Techniques is a Transformative Journal (TJ). Authors may publish their research with us through the traditional subscription access route or make their paper immediately open access through payment of an article-processing charge (APC). Authors will not be required to make a final decision about access to their article until it has been accepted.

Authors may need to take specific actions to achieve compliance with funder and institutional open access mandates. If your research is supported by a funder that requires immediate open access (e.g. according to Plan S principles) then you should select the gold OA route, and we will direct you to the compliant route where possible. For authors selecting the subscription publication route our standard licensing terms will need to be accepted, including our self-archiving policies. Those standard licensing terms will supersede any other terms that the author or any third party may assert apply to any version of the manuscript.

Find out more about compliance https://www.springernature.com/gp/open-research/funding/policy-compliance-faqs

Thank you for your fine contribution. On behalf of the Editors of Nuclear Science and Techniques, we look forward to your continued contributions to the Journal.

Sincerely,
Dr. Yugang Ma
Editor-in-Chief
Nuclear Science and Techniques

Optimization of the FRIB Beam Dump: A Hybrid Genetic Algorithm and Reinforcement Learning Approach

Geunhyeong Lee*, Jeongseog Song, Raul Quispe-Abad, Mohit Patil, Takuji Kanemura

Facility for Rare Isotope Beams, Michigan State University, East Lansing, MI, USA

*Corresponding author. *E-mail address:* leeg@frib.msu.edu

Abstract

The operational performance of high-power density systems, such as particle accelerators and next-generation nuclear reactors, is critically limited by the challenge of managing extreme thermal loads. To address this, we present a novel hybrid optimization framework combining a Genetic Algorithm (GA) with a Soft Actor-Critic (SAC) deep reinforcement learning agent. This framework was applied to a demanding real-world problem: redesigning the beam dump at the Facility for Rare Isotope Beams (FRIB) for a power upgrade from 20 kW to 50 kW. The resulting design, validated by 3D simulations, eliminates hazardous hot spots and achieves a highly uniform temperature distribution. This provides a robust operational margin, increasing the average power-handling capability by 72% over the current design, showcasing the framework's potential to solve complex thermal management challenges in both accelerator technology and advanced nuclear systems.

Keywords Heat removal system, Beam dump, Optimization, Genetic Algorithm, Reinforcement Learning, Heat exchanger, Accelerator, FRIB.

Introduction

Designing components for extreme thermal conditions is a critical challenge in advanced engineering fields, particularly for high-power density systems like particle accelerators and nuclear reactors [1], [2]. In these environments, the ability to efficiently manage heat is a primary factor limiting performance and technological progress. High-power particle accelerators, such as the Facility for Rare Isotope Beams (FRIB), serve as an ideal case study for this challenge. At FRIB, the unreacted primary beam is directed into a beam dump, a critical component designed to safely absorb and dissipate immense energy to prevent material failure [3]. This component is the primary bottleneck in FRIB's planned power ramp-up from 20 kW to 50 kW, as the current design cannot mitigate the formation of hazardous hot spots at higher power levels. Overcoming this requires a shift from traditional, experience-based improvements to systematic optimization methods that can navigate complex design spaces to find robust, global optima [4].

High-power particle accelerators, such as the Facility for Rare Isotope Beams (FRIB), represent one of the most demanding environments for thermal management. As shown in Fig. 1, the unreacted primary beam at FRIB is directed into a beam dump, a critical component designed to safely absorb and dissipate this immense energy to prevent material failure [4].

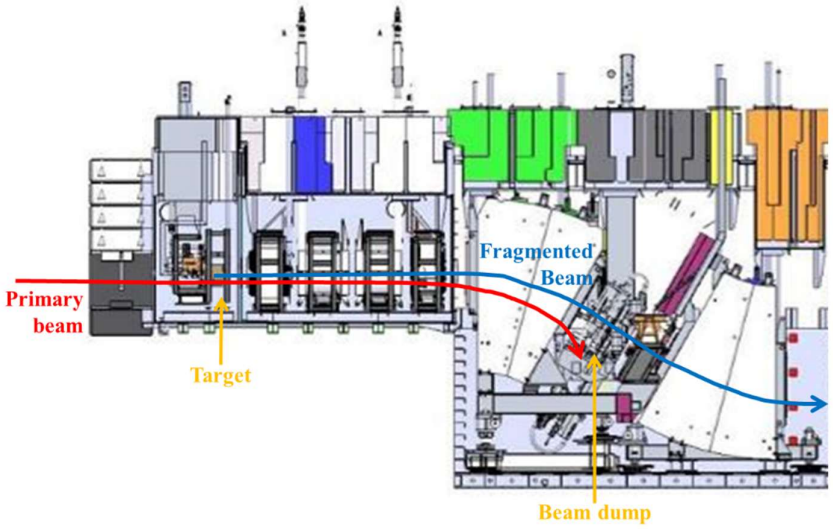

Fig 1. FRIB Target hall

The beam dump plays a critical role in stopping the beam and is considered the most challenging system in FRIB's planned power ramp-up from 20 kW to 50 kW [5]. This challenge arises primarily from the heavy ion beams, such as ^{238}U, accelerated at FRIB. Unlike proton beams, these heavy ions possess a high atomic number (Z) and consequently exhibit a stopping power approximately three to four orders of magnitude higher than that of protons. As a result, the beam energy is deposited within an extremely small volume near the surface with a negligible penetration depth. This characteristic makes direct water cooling challenging, as it would require a dangerously thin window (approximately 1 mm); therefore, a solid absorber approach is applied. Dissipating 50 kW of heat concentrated on this solid absorber imposes a severe thermal load. Notably, due to this distinct surface heating mechanism, this 50 kW heavy ion load induces peak thermal stresses comparable to a volumetric proton beam load of significantly higher power. Consequently, spreading the beam's energy over a large area to keep local temperatures below material damage limits is a critical requirement.

To manage these high thermal loads, FRIB currently achieves this by directing the beam at a shallow 6° incidence angle onto a water-cooled dump, which lengthens the beam's path and reduces the power deposition. The absorber plate incorporates a CuCrZr copper alloy bonded to Al 2219 through explosion bonding, has 2 mm × 7 mm water channels, and features 3D-printed wings made from AlSi10Mg, as shown in Fig. 2 [6].

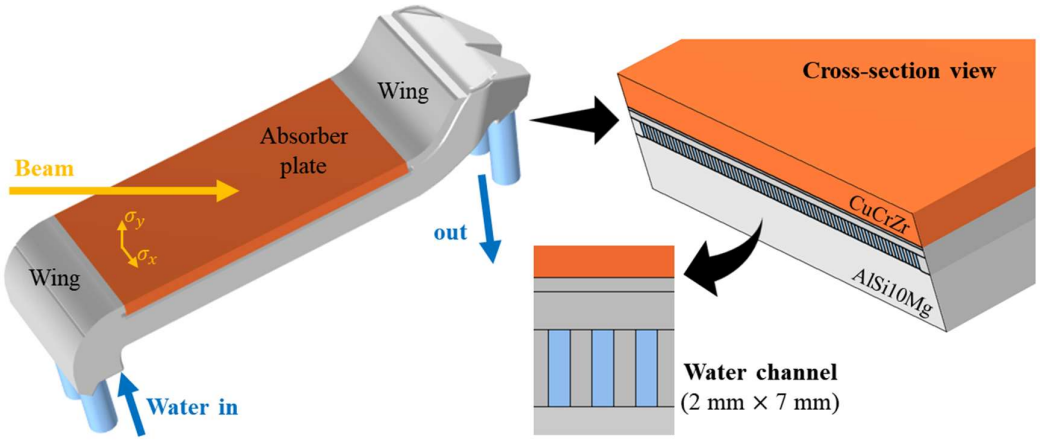

Fig 2. Current FRIB beam dump design

However, this existing design is insufficient for the required 50 kW operation. The primary objective is to prevent excessive localized heating (hot spots) by re-distributing the energy deposition more evenly across the dump surface. This is a complex multi-variable optimization problem, as the design must perform robustly across a range of operational beam sizes and satisfy manufacturing constraints. Traditional trial-and-error engineering methods struggle in this high-dimensional design space and cannot efficiently find a global optimum. Therefore, advanced optimization techniques are required to solve this challenge.

A powerful and widely used method for solving such engineering optimization problems is the Genetic Algorithm (GA) [7]. GAs conduct a global search by mimicking evolutionary processes, enabling them to navigate large design spaces and handle non-linear, multi-objective problems. They have been widely applied in engineering for their ability to escape local minima and discover efficient solutions [8]. For the thermal-hydraulic approach, recent genetic algorithm (GA) studies have demonstrated effectiveness across various thermo-fluid engineering applications. Garcia et al. [9] optimized microchannel heat exchangers, achieving volume and fan power reductions by up to 45% and 51%, respectively. Zhang et al. [10] applied GA optimization to elliptical tube fin heat exchangers, successfully reducing pressure drop by 20% without compromising heat transfer efficiency. Jin et al. [11] optimized zigzag parameters in printed circuit heat exchangers for supercritical CO_2 Brayton cycles, significantly lowering pressure drop. Meng et al. [12] utilized GA to enhance plate heat exchanger designs for commercial electric vehicles, improving the comprehensive performance factor by approximately 21.5%. Hamed et al. [13] employed GA optimization on inserted coiled tube three-fluid heat exchangers to minimize entropy generation effectively. Additionally, Mekki et al. [14] used GA-driven topology optimization to achieve performance improvements of up to 89% in aerospace fin structures. Moon et al. [3] combined metal additive manufacturing with GA optimization, resulting in ultra-power-dense heat exchangers exhibiting specific power roughly twentyfold higher than commercial counterparts.

However, the effectiveness of a pure Genetic Algorithm (GA) approach is constrained by several limitations. A primary concern is the risk of premature convergence, where the algorithm gets trapped in a local, suboptimal solution instead of finding the global optimum [13], [15]. These challenges are often exacerbated in high-dimensional design spaces. GAs are inherently multi-dimensional methods involving complex interactions among their parameters, which become increasingly difficult to manage as the number of variables grows. In such large-scale problems, the algorithm can be overwhelmed, In other words, the GA might find a good rough configuration of the beam dump, but fine-tuning the shape for ideal thermal performance would be difficult using a GA alone. This is where reinforcement learning (RL) offers a powerful complement to GA-based design.

RL algorithms excel at iteratively improving a solution by learning from interactions with a simulation or environment, gradually maximizing a defined performance reward. They have shown great promise in complex systems through trial-and-error learning. For recent thermo-fluid problems, RL has been successfully applied in various heat transfer optimization scenarios. Keramati et al. [16] used deep reinforcement learning (DRL) coupled with computational fluid dynamics (CFD) to optimize heat exchanger shapes, significantly enhancing heat transfer performance while reducing pressure drop. Similarly, Wang et al. [17] demonstrated the feasibility of DRL for forced convection control, achieving superior cooling performance compared to traditional control methods. Ortiz-Mansilla et al. [18] employed RL to optimize near-field radiative heat transfer between multilayer hyperbolic metamaterials, showing that RL-driven methods could outperform traditional intuition-based optimization. Hachem et al. [19] introduced a novel RL technique using proximal policy optimization (PPO) for controlling conjugate heat transfer problems, effectively improving thermal homogeneity across complex geometries. Additionally, Wang et al. [20] integrated DRL with PID control strategies, significantly enhancing temperature tracking accuracy in indirect-contact heat exchangers within energy systems, demonstrating robustness under varying operational conditions. Li et al. [21] proposed a distributed DRL framework to handle multi-objective heat management in proton exchange membrane fuel cells, effectively coordinating multiple control objectives and significantly improving operational efficiency. Lee et al. [22], [23] presented a DRL-based topology optimization for printed circuit heat exchangers

(PCHEs), achieving notable enhancements in thermal performance, and demonstrated the practicality of these optimized designs through 3D printing technology.

Especially when combined with thermal simulation that requires extensive computational resources, the Soft Actor-Critic (SAC) algorithm has merits for this application. SAC is an advanced off-policy deep RL algorithm that optimizes a stochastic policy with an entropy-maximization objective [24]. Practically, this means it can efficiently reuse past simulation experiences via a replay buffer and maintain excellent sample efficiency that is a critical feature when each function evaluation is computationally expensive [25], [26].

Building upon our preliminary study [27], which demonstrated the initial feasibility of the hybrid concept, this work proposes an advanced optimization framework. This approach combines the global search strengths of a GA with the fine-tuning capabilities of RL to redesign the FRIB beam dump for 50 kW operation. Our framework employs a two-stage process: first, a Genetic Algorithm explores the broad geometric design space to identify a promising baseline configuration. Subsequently, a Soft Actor-Critic (SAC) agent interacts with a thermal simulation of this baseline design, making localized adjustments to refine the geometry. The specific objective is to minimize the maximum surface temperature across several representative beam conditions, thereby ensuring a robust design that can safely dissipate the increased beam power without hot-spot failures. The following sections describe the development and results of this hybrid optimization in detail, demonstrating the power of combining GA and RL for solving complex thermo-fluid engineering problems in the accelerator domain.

Method

To address the complex, multi-variable challenge of redesigning the beam dump, a two-stage hybrid optimization framework was developed. This approach synergistically combines a Genetic Algorithm (GA) for robust global exploration with a deep Reinforcement Learning (RL) agent for high-fidelity local refinement. The core strategy is to leverage the distinct strengths of each algorithm: the GA's

ability to efficiently navigate a vast design space to identify promising baseline configurations, and the RL agent's capacity for precise, data-driven fine-tuning to converge on a final, high-performance design. This hybrid process is more effective and computationally efficient than using either method in isolation, as it balances broad exploration with precise exploitation.

The overall workflow is sequential, as depicted in Figure 3. The process commences with the GA performing a broad search over a set of 13 coarse geometric parameters to identify a globally promising design region. The best-performing individual from the GA's final population, determined by evaluating the negative of the maximum temperature as the fitness score, is then used as the starting point for the second stage. In this stage, a Soft Actor-Critic (SAC) reinforcement learning agent interacts with a thermal simulation of the design. The agent, whose policy is informed by a Convolutional Neural Network (CNN) processing the temperature field as input, makes iterative, localized adjustments to 34 fine-tuning surface points to further minimize the peak temperature. This iterative refinement continues for 500 episodes, with the agent learning to maximize a reward signal correlated with temperature reduction. The used Finite Difference Method (FDM) simulation was validated by the COMSOL simulation to confirm performance and calculated power limits.

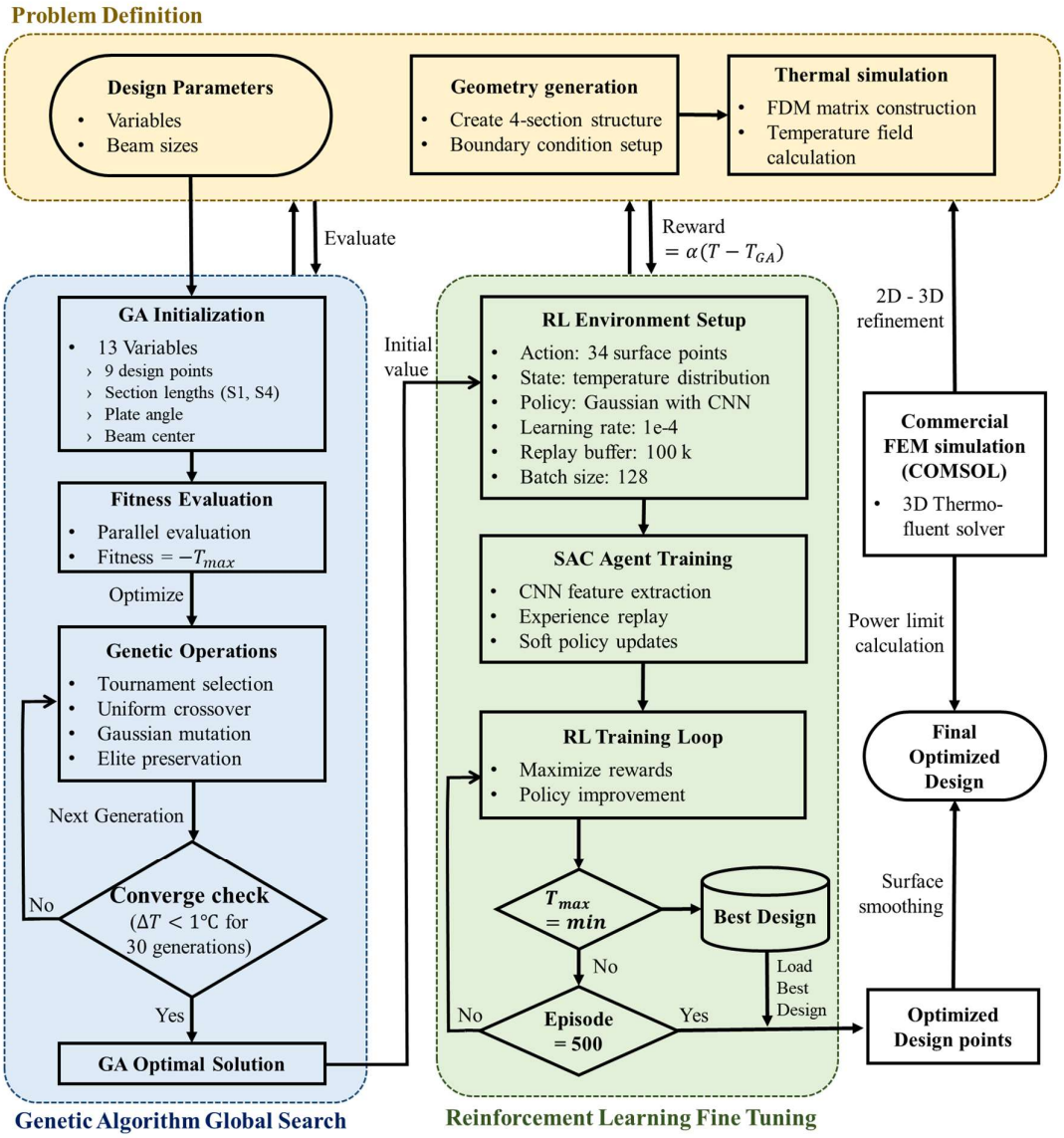

Fig 3. Overall Optimization Process

Problem definition

The primary optimization goal is to minimize the maximum temperature within the beam dump structure across a set of representative operational beam conditions. The analysis was performed for a ^{238}U beam accelerated to 177 MeV/u. Considering the interaction with a graphite target thickness of 2.1 mm, 63.3% of the primary beam power is deposited into the beam dump. The beam's geometric distribution, defined by its size (σ_x, σ_y), varies significantly depending on the beam's magnetic rigidity

deviation, as illustrated in Fig. 4. The operation curve was established as the reference by selecting a path between two potential optics to avoid extreme beam size variations.

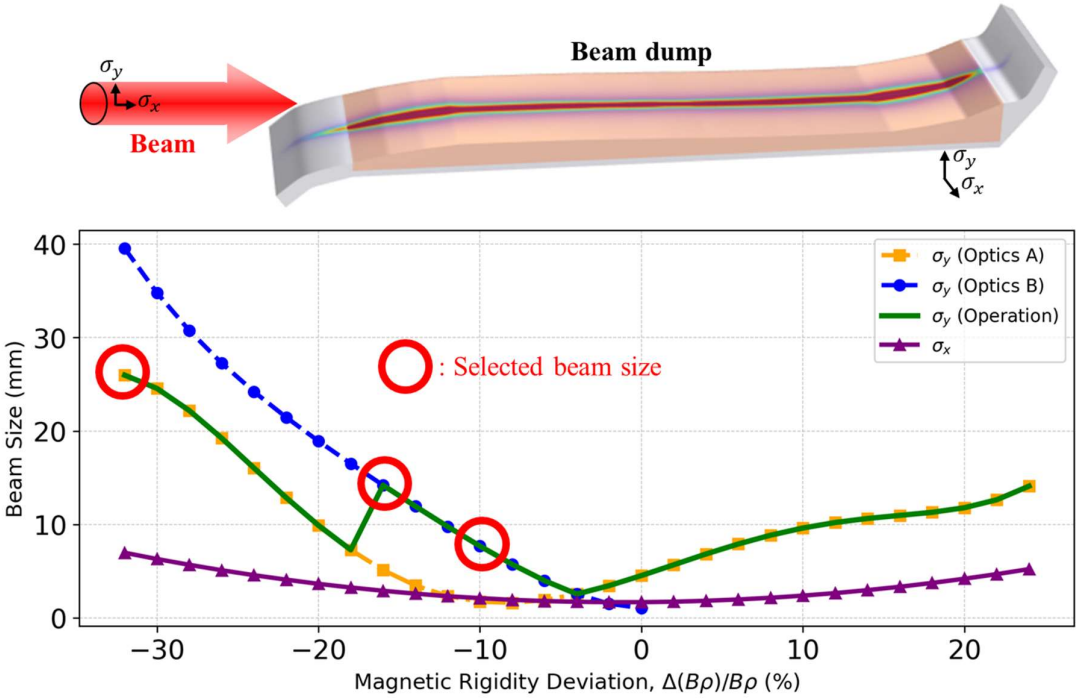

Fig. 4. Beam spot and beam size selection

The DRL stage requires a separate FDM simulation for each beam spot at every training step, making the optimization time highly dependent on the number of cases. Therefore, to ensure the design is robust for the 50 kW upgrade across a wide operation range [27], we selected three representative beam size pairs. The selected cases, highlighted by red circles in Fig. 4, were chosen to cover the critical operational boundaries: (6.97, 25.98) mm (representing the largest operational spot), (2.9, 14.2) mm (a key intermediate spot), and (2.11, 7.68) mm (representing the smallest spot logically feasible for 50 kW operation).

The cooling water system is designed to manage the high thermal load using 32°C water supplied at a total flow rate of 60 GPM. To optimize cooling efficiency, the flow passage is divided into distinct zones based on the heat deposition profile. In the central beam impact area (Section 2 and 3 in Fig. 5), the water is directed through 42 mini-channels, each 2 mm wide and 7 mm high as detailed in Fig. 2.

This geometry accelerates the flow to an average velocity of 6.4 m/s to maximize heat transfer performance. In contrast, the wing regions (Section 1 and 4 in Fig 5) experience lower thermal loads and therefore utilize a 10 mm thick bulk channel without the mini-channel structure. This configuration replicates the geometry of the currently operational beam dump (Fig. 2) and is fully compatible with existing additive manufacturing capabilities, ensuring the design's technical soundness and fabricability.

To make the optimization computationally manageable with less time for GA and RL algorithm, the three-dimensional geometry of the beam dump was simplified into a two-dimensional cross-sectional model. The 2D model, shown in Figure 5, is divided into four sections: Sections 1 and 4 consist of 3D-printed wings, while Sections 2 and 3 comprise a bi-metal plate. The design retains the previous water channel configuration, with a length of 600 mm and a height of 140 mm, constrained by the space available in the FRIB beam dump area. The prescribed material thicknesses are set to avoid exceeding the boiling point of the cooling water: 15 mm for CuCrZr, 5 mm for Al 2219, and 12 mm for AlSi10Mg. Furthermore, the maximum allowable temperature for both Cu and Al alloys is limited to 350℃ to prevent material degradation. The changeable variables from the GA are 9 design points, section 1 length, section 4 length, plate angle, and beam center location. The changeable variables from the RL is 34 surface points including GA design points and RL design points. The geometry is formatted by the prescribed value and changeable variables as Fig 5.

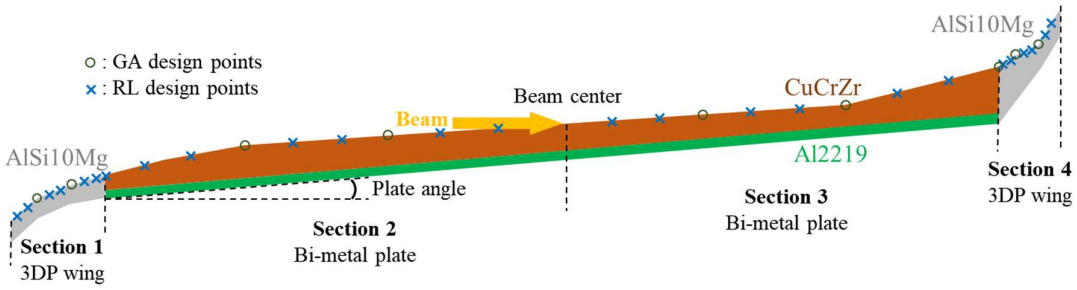

Fig 5. Schematic of the geometry used for simulation

The thermal performance of each candidate design is evaluated using a custom 2D thermal solver developed in Python. The solver is built upon the FDM to solve the steady-state heat conduction equation in a two-dimensional domain representing the beam dump's cross-section.

For the material's internal domain, the governing equation is the source-free steady-state heat conduction equation:

$$\nabla \cdot (\mathrm{k}(\mathrm{x},\mathrm{y})\nabla \mathrm{T}(\mathrm{x},\mathrm{y})) = 0$$

Here, $\mathrm{T}(\mathrm{x},\mathrm{y})$is the temperature field, $\mathrm{k}(\mathrm{x},\mathrm{y})$ is the position-dependent thermal conductivity. The thermal conductivities for the materials were defined as constants at temperature limit (350 ℃ [5]) for simple calculation: 354 $\mathrm{W/mK}$ for CuCrZr [28], 158 $\mathrm{W/mK}$ for Al2219 [29], and 170 $\mathrm{W/mK}$ for AlSi10Mg [30].

The domain is discretized into a grid with 0.5 mm spacing. For an internal node (i,j), this equation is discretized using a five-point stencil FDM scheme. The thermal conductivity k at the interface between nodes is calculated using a harmonic mean to accurately handle material interfaces.

For nodes located on the boundaries, the standard FDM equation is replaced with specific boundary condition equations that model heat exchange with the surroundings. The top surface experiences a complex condition involving both heat gain from the beam and heat loss from out-of-plane conduction, governed by the energy balance equation:

$$-\mathrm{k}\frac{\partial T}{\partial n} = h_{upper}\left(T_{surf} - T_{water}\right) - \mathrm{q}_{beam}$$

The term q_{beam} represents the incoming heat flux from the particle beam, whose magnitude depends on a Gaussian profile and the angle of incidence. To compensate for the 2D model's inability to represent out-of-plane heat dissipation, an equivalent heat transfer coefficient, h_{upper}, is applied. This coefficient is calculated using the empirical relation $\mathrm{h}_{upper} = C \cdot k_{local}/\sigma_x^p$, where C and p are section-dependent constants.

The bottom surface is cooled by forced convection, a simpler Robin boundary condition where heat is removed:

$$-\mathrm{k}\frac{\partial T}{\partial n} = h_{cool}(T_{surf} - T_{water})$$

Here, h_{cool} is the heat transfer coefficient and T_{water} is the coolant temperature, set to 32°C. To reflect manufacturing constraints, the vertical interfaces between sections S1-S2 and S3-S4 are modeled as adiabatic, where no heat conduction occurs (∂T/∂n=0).

This complete system of discretized equations for both internal and boundary nodes is assembled into a sparse matrix equation, AT = b, which is solved to find the temperature vector T.

Genetic Algorithm for Global Search

The initial global search phase was conducted using a Genetic Algorithm (GA), specifically configured to explore the design space of the beam dump geometry. Each potential design is represented by a chromosome, which is a real-valued vector of 13 parameters. These parameters encode the coarse geometric features: four variables defining S1 and S4 section lengths, the bi-metal plate angle, and the horizontal beam offset, supplemented by nine free y-coordinates that define the initial surface curvature shown in Fig 5. An initial population of 100 individuals was generated by randomly sampling each parameter within its predefined constraints.

The fitness of each individual was quantified based on its worst-case thermal performance to ensure the robustness of the final design. The custom FDM solver evaluated each geometry against all three representative beam sizes, and the fitness score was defined as the negative of the single highest peak temperature recorded across these simulations. This formulation transforms the temperature minimization problem into a fitness maximization task suitable for the GA. To manage the computational demand of this step, the fitness evaluations for the population were executed in parallel.

The population evolved over a maximum of 500 generations, driven by a set of carefully chosen genetic operators. At each generation, a tournament selection scheme with a tournament size of three was employed to select parent chromosomes for reproduction. New offspring were subsequently generated using uniform crossover with a probability of 0.9, where traits from two parents are exchanged on a gene-by-gene basis [31]. These offspring then underwent Gaussian mutation with a probability of 0.12, introducing small, normally distributed variations to the parameters to facilitate fine-tuning and prevent premature convergence [32]. An elitism strategy was also implemented, ensuring that the four best-performing individuals from the current generation were automatically carried over to the next, preserving the best-found solutions throughout the evolutionary process. The

algorithm terminates upon reaching the maximum generation count or if the solution converges, which is defined as an improvement in the best temperature of less than 1°C over 30 consecutive generations.

Reinforcement Learning for Fine Tuning

Following the global search, the optimal design from the GA was passed to a Soft Actor-Critic (SAC) agent for high-fidelity refinement [25]. The state provided to the agent is the complete 2D steady-state temperature field from the FDM simulation. This thermal data is represented as an image-like tensor and processed by a Convolutional Neural Network (CNN) that serves as a shared feature extractor [33]. The CNN consists of three convolutional layers with ReLU activation, which transforms the spatial temperature distribution into a compressed feature vector for the actor and critic networks.

The action (A) is a continuous vector of 34 elements, where each element defines a small vertical adjustment, Δy, to a specific point on the beam dump surface. These 34 fine-tuning points are generated by expanding the initial geometry provided by the GA. For each of the four surface sections, additional points are interpolated between the original design points, creating a higher-resolution profile for the RL agent to manipulate. To ensure the physical validity of the geometry and prevent self-intersecting surfaces, a monotonic constraint is enforced on the y-coordinates after each action is applied. This approach allows the agent to make precise, localized modifications while maintaining a viable geometric shape inherited from the GA's global search.

The reward function was designed to provide a dense and informative feedback signal based on the temperature improvement relative to the GA's best result ($T_{max,GA}$). Given the peak temperature after an agent's action ($T_{max,RL}$), the change $\Delta T = T_{max,GA} - T_{max,RL}$ is calculated. An asymmetric reward structure was implemented to strongly incentivize improvements: if the action results in a lower temperature ($\Delta T > 0$), the reward is positively scaled and a significant bonus is added; otherwise, the reward is scaled with a smaller penalty factor. This structure encourages the agent to discover superior solutions while allowing for effective exploration.

The SAC agent was implemented with a twin-critic architecture to mitigate Q-value overestimation and was trained for 500 episodes with 10 steps [34]. All networks, including the actor, critics, and the

shared CNN encoder, were updated using the Adam optimizer with a learning rate of 1×10^{-4} [35]. Training transitions were sampled in mini-batches of 128 from a replay buffer with a capacity of 100,000 experiences, an off-policy approach that enables efficient reuse of computationally expensive simulation data. The entropy regularization coefficient (α), a key SAC hyperparameter that balances the exploration-exploitation trade-off, was set to a fixed value of 0.02 throughout the training process.

3D Simulation and validation

To validate the thermal performance of the final optimized geometry under realistic three-dimensional conditions, a 3D conjugate heat transfer (CHT) simulation was performed. The thermal boundary conditions were consistent with those described in the Problem Definition section, while the fluid dynamics were modeled using a k-ε turbulence model, with a water flow rate of 60 GPM at the inlet and pressure outlet condition.

Prior to the main analysis, a mesh independence study was conducted to ensure the numerical accuracy and computational efficiency of the model. As illustrated in Fig. 6, the maximum temperature was calculated for several mesh densities using the objective beam sizes. Based on this study, a mesh with 924,323 elements was selected, as it provided a balance between precision and computational cost, yielding a temperature deviation of less than 1.4% compared to a finer mesh with over 6.4 million elements.

Furthermore, the simulation methodology was validated against experimental results by Song et al [36]. A thermal simulation of the current beam dump shown in Fig. 2 was conducted and compared with experimental test data. The experiment utilized a 17 keV electron beam to replicate a 15 kW deposited power scenario (75% of 20 kW primary beam power operation). The validation test was performed with a 40 GPM water flow rate and a 30°C inlet temperature. The results showed strong agreement, with discrepancies between the simulated and measured surface temperatures within ±5%, which confirms the predictive reliability of the thermal model used in this work.

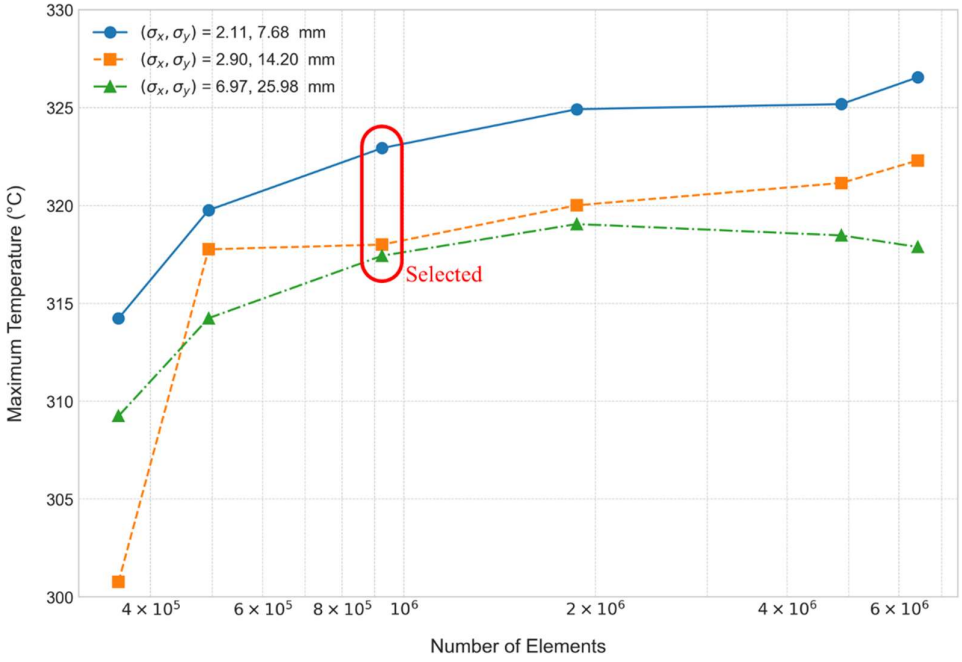

Fig 6. Mesh independent simulation results

Results

The hybrid optimization approach produced an improved geometry for the FRIB beam dump, leading to a significant reduction in peak temperature. The first stage of this process, the Genetic Algorithm (GA) optimization, is illustrated in Figure 7. The optimization history shows a clear convergence trend, with the maximum temperature of the best-performing design dropping from an initial value of 554.7 °C. As the generations progressed, the GA iteratively refined the beam dump's geometry to minimize the worst-case temperature across all specified beam sizes. The scattered points in Figure 7 represent the maximum temperatures for each of these cases, indicating that the algorithm successfully found a robust design that performs well under various conditions. After converging in 107 generations, the GA stage concluded, achieving a final optimized maximum temperature of 345.9 °C.

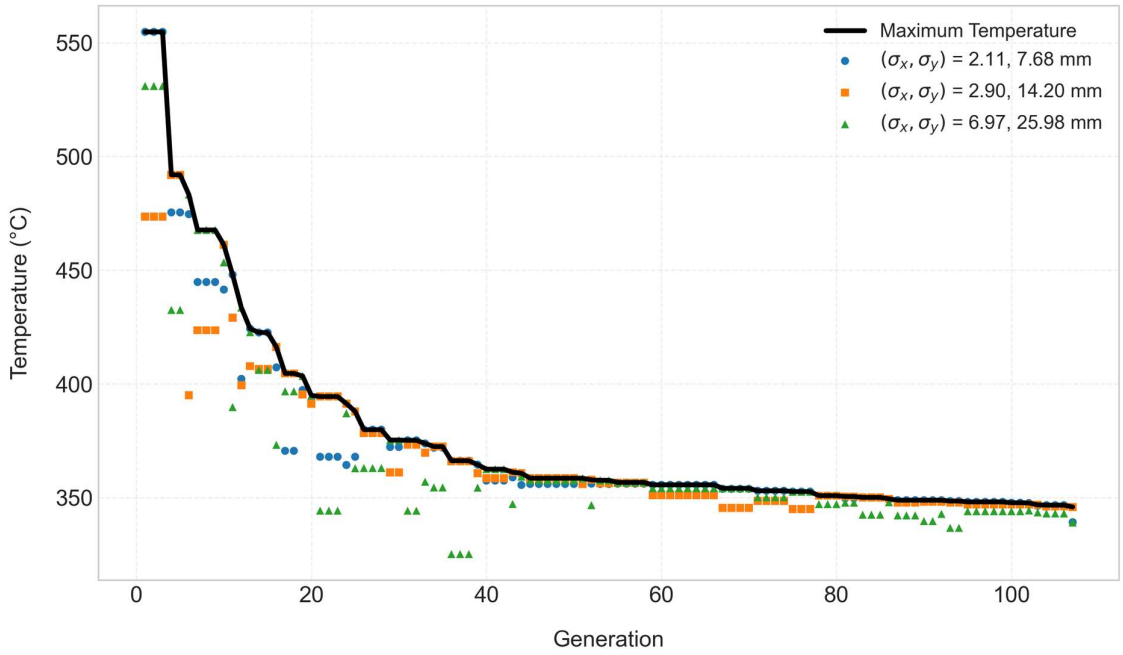

Fig. 7. Genetic algorithm optimization temperature trend by generation

To further refine the global optimum design identified by the Genetic Algorithm, a Soft Actor-Critic (SAC) deep reinforcement learning agent was employed for local geometry optimization. The primary objectives were to minimize the peak temperature and create a more uniform temperature distribution on the beam dump surface. Figure 8 illustrates the training history of the SAC agent over 500 episodes. The x-axis represents the training episode, while the y-axes show the reward and maximum temperatures under various beam conditions. As training progresses, the reward exhibits a clear upward trend, indicating that the agent successfully learned an effective policy to improve thermal performance.

Concurrently, the overall maximum temperature was successfully reduced by 21.8 °C from the GA-optimized baseline of 345.9 °C to a final value of 324.1 °C. This final optimized state yielded maximum temperatures of 324.1 °C, 319 °C, and 321 °C for beam sigma (σ_x, σ_y) pairs of (2.11, 7.68) mm, (2.9, 14.2) mm, and (6.97, 25.98) mm, respectively.

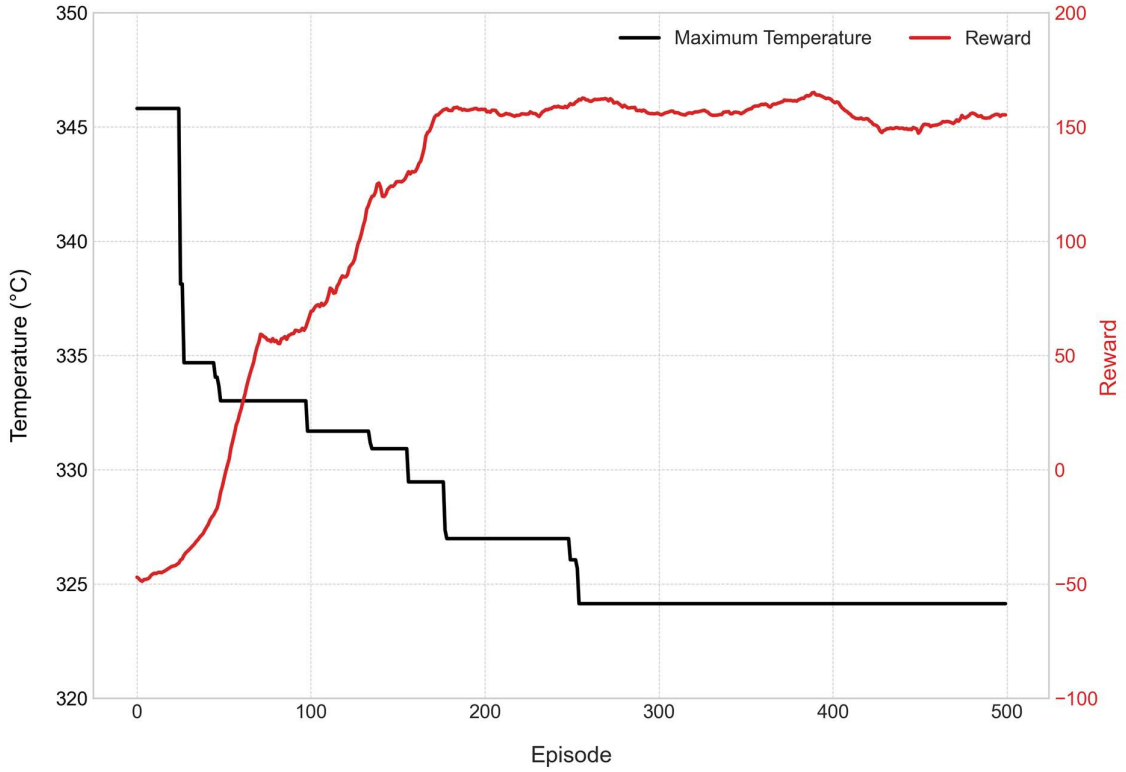

Fig. 8. Reinforcement learning temperature and reward trend by episode

Figure 9 provides a visual comparison between the current beam dump design and the optimized geometry for 50 kW operation achieved through the hybrid genetic algorithm and reinforcement learning, with the final design constrained within the predefined boundary (r = 368.3 mm). The final optimized parameters are a section 1 length of 58.4 mm, a section 4 length of 30 mm, a plate angle of 4.66°, and a beam center located at 324.1 mm. The optimized design features a shallower plate angle compared to the initial design's inferred angle of 6°. This reduction in the plate angle, while effectively utilizing the available design space, facilitates a more gradual deceleration of the beam particles, thereby contributing to a wider distribution of the deposited heat and a reduction in the peak temperature.

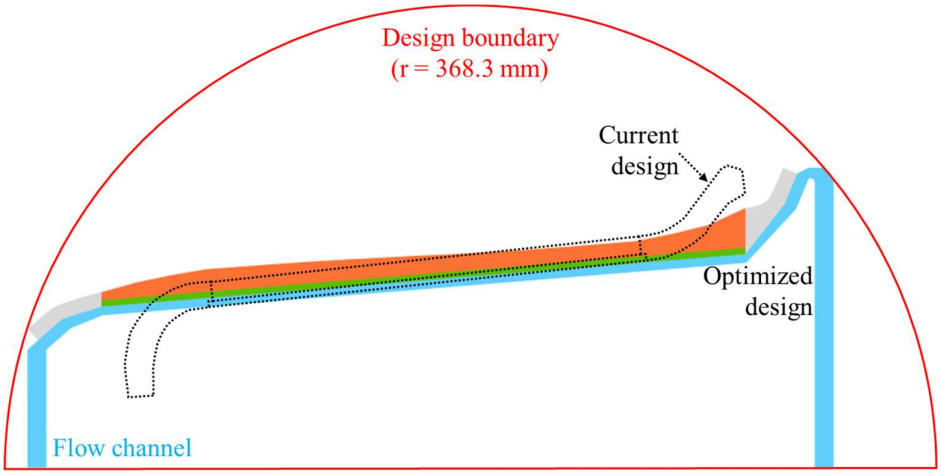

Fig. 9. Geometrical comparison between current design and optimized design within design boundary

The thermal performance of the optimized geometry is visually demonstrated in Figure 10, which presents a comparative 3D CHT analysis of the surface temperature distributions between the current and optimized designs under three distinct operational beam conditions. In the current design, the beam energy creates highly localized thermal loads, resulting in significant hot spots with a maximum temperature reaching as high as 688.5 °C for the (σx, σy) = (6.97, 25.98) mm beam case. In stark contrast, the optimized design effectively mitigates these peak temperatures, reducing them to 324.9 °C, 320 °C, and 319.1 °C for the respective beam sizes. Notably, these temperatures obtained from the comprehensive 3D simulation show good agreement, within 1%, with the final values predicted by the 2D FDM model in the RL optimization phase (324.1 °C, 319 °C, and 321 °C, respectively), confirming the high fidelity of the simplified model used for optimization. Consequently, the heat load is spread more evenly along the beam's path, eliminating the hazardous hot spots and validating the success of the hybrid optimization framework.

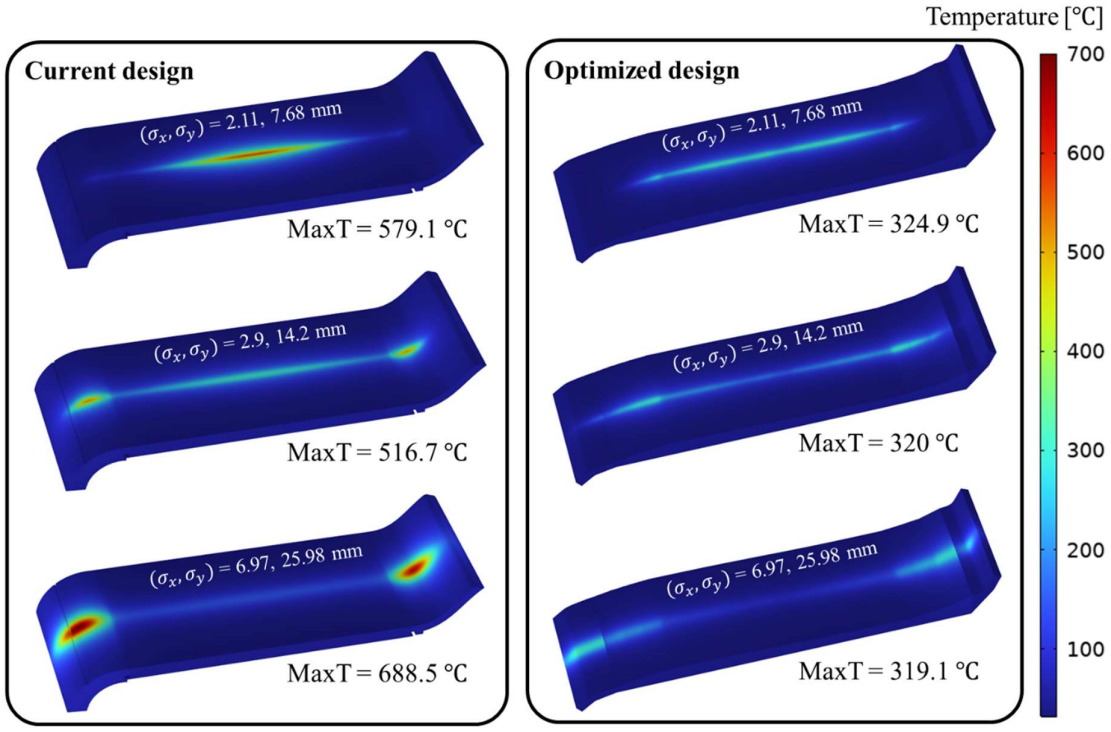

Fig. 10. Comparison of surface temperature distributions between the current and optimized beam dumps

To understand the thermal behavior better, the heat flux distribution on the beam dump surface is analyzed in Fig. 11. In the current design, for the small beam size (2.11 mm, 7.68 mm), the deposited heat is highly concentrated at the center due to the geometric configuration. For the large beam size (6.97 mm, 25.98 mm), the heat flux on the wing section is significant. This results in high temperatures because this region lacks the mini-channel structure for enhanced cooling. The optimized design intelligently distributes the heat load matching the local cooling capacity, outperforming the current design. In the central region, where the mini-channels provide efficient cooling, the design allows a high heat flux of 1300 W/cm^2 at the small beam size. Conversely, in the wing regions, where the cooling is less efficient, the heat flux is distributed at a lower level of 550 W/cm^2 at the large beam size. This strategic distribution explains why the maximum temperature remains stable despite the variations in beam conditions.

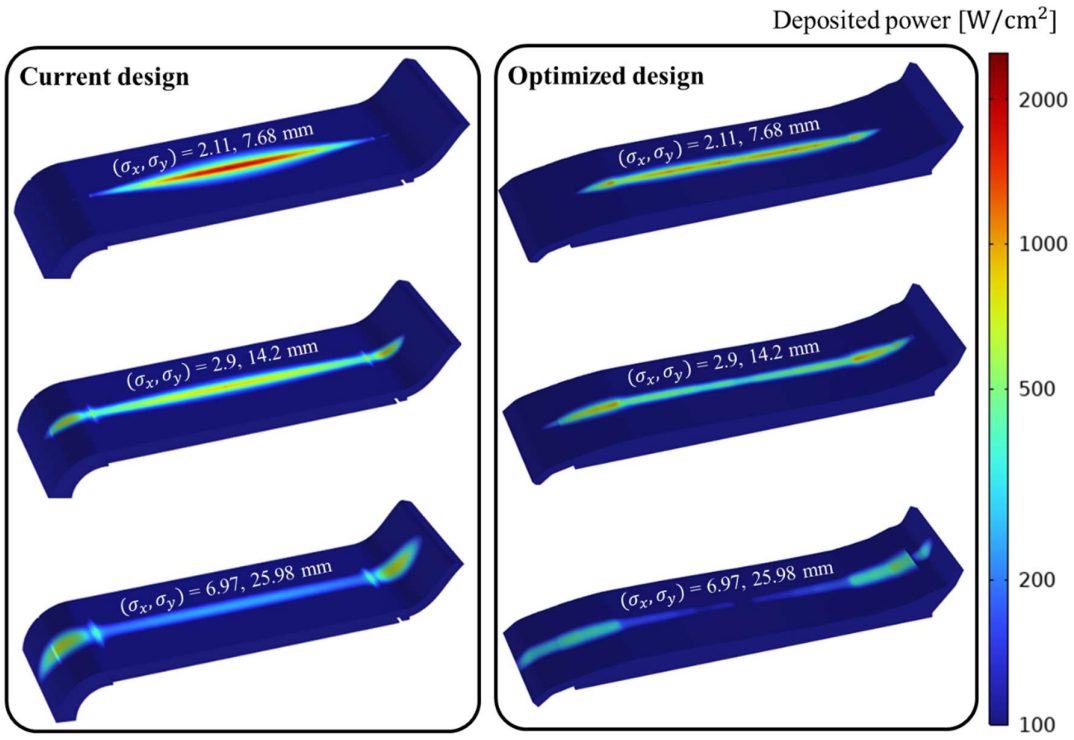

Fig 11. Comparison of log-scaled deposited power density distributions on the current and optimized beam dumps

Building on this enhanced thermal stability, Figure 12 illustrates the practical impact on the beam dump's operational envelope. The top panel plots the primary beam power limit as a function of magnetic rigidity deviation, and the bottom panel shows the corresponding operation beam sizes from Fig. 4. The power limit was calculated based on the constraint that the maximum material temperature does not exceed 350 °C. The results show that the optimized design possesses a substantially higher power handling capability across the entire range of magnetic rigidity deviations compared to the current design. Notably, the optimized beam dump consistently meets or exceeds the FRIB's required 50 kW power limit for most operating conditions, whereas the current design's capability remains well below this threshold. This significant improvement confirms that the new design provides a robust operational margin, achieving an average power-handling capability increase of 72% that was calculated by averaging the percentage increase in the power limit across the entire range of magnetic rigidity deviations.

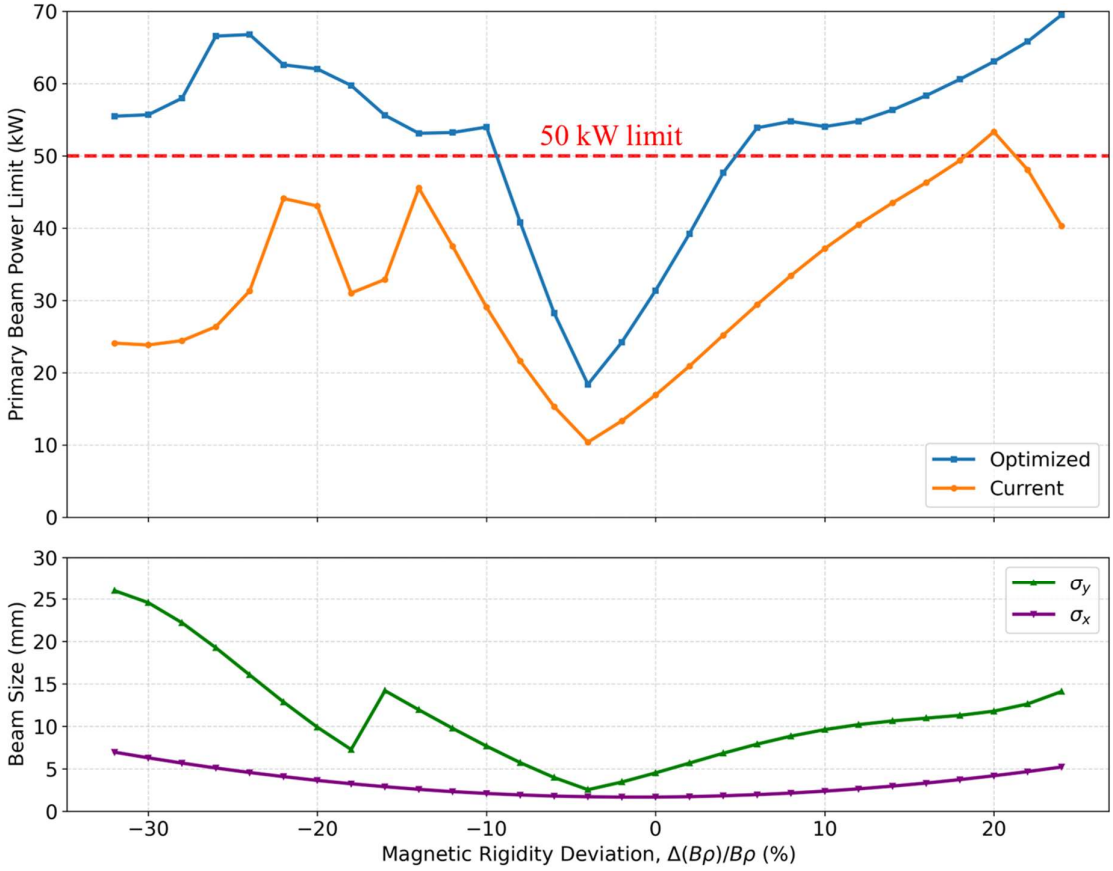

Fig. 12. Primary beam power limits of the current and optimized beam dumps at 350℃ material temperature limit

Conclusion

This study successfully demonstrated a novel hybrid optimization framework combining a G enetic Algorithm (GA) with Soft Actor-Critic (SAC) reinforcement learning to redesign the F RIB beam dump for an upgraded 50 kW operation. The two-stage approach effectively levera ged the strengths of each method: the GA performed a robust global search to identify a pro mising design envelope, while the SAC agent conducted high-fidelity local refinement to fine-tune the surface geometry.

The resulting optimized design achieved the primary objectives of this work. 3D conjugate heat transfer simulations confirmed a significant reduction in peak operational temperatures, wi th hazardous hot spots being effectively eliminated across a range of representative beam con ditions. The optimized geometry promotes a more uniform surface temperature distribution by enhancing heat spreading along the beam's path.

Crucially, this thermal performance enhancement translates into a substantial improvement in the beam dump's operational capabilities. The new design meets the required 50 kW power-handling threshold across a wide spectrum of 238U beam magnetic rigidity deviations, providing a robust operational margin that the original design lacked. This represents an average power-handling capability increase of 72%.

In summary, this work demonstrates that a high-performance beam dump can be fabricated based on this validated design. Furthermore, it establishes a powerful and efficient optimization methodology that can be readily adapted to solve similar complex, multi-variable thermal management challenges in other high-power accelerator components and advanced heat removal systems.

Acknowledgement

This material is based upon work supported by the U.S. Department of Energy, Office of Science, Office of Nuclear Physics and used resources of the Facility for Rare Isotope Beams (FRIB) Operations, which is a DOE Office of Science User Facility under Award Number DE-SC0023633.

Declaration of interests

The authors declare no competing interests.

Data availability statement

The datasets generated during and/or analyzed during the current study are available from the corresponding author on reasonable request

References

1 J.H. Lim, S.H. Yu, A historical review of high heat flux cooling techniques. Nucl. Eng. Technol. **57**, 103725 (2025). doi:10.1016/j.net.2025.103725

2 N. Lee, B.S. Kim, H. Moon, J.-S. Lim, H.H. Cho, Heat-Absorbing Capacity of High-Heat-Flux Components in Nuclear Fusion Reactors. Energies **12**, 3771 (2019). doi:10.3390/en12193771

3 J. Wei et al., FRIB operations: first three years. in *16th International Conference on Heavy Ion Accelerator Technology (HIAT2025)* (2025). doi:10.18429/JACoW-HIAT2025-MOX01

4 H. Moon, D.J. McGregor, N. Miljkovic, W.P. King, Ultra-power-dense heat exchanger development through genetic algorithm design and additive manufacturing. Joule **5**, 3045–3056 (2021). doi:10.1016/j.joule.2021.08.004

5 S. Miller et al., Optimization of a mini-channel beam dump for FRIB operation. in *16th International Conference on Heavy Ion Accelerator Technology (HIAT2025)* (2025). doi:10.18429/JACoW-HIAT2025-TUP01

6 J. Song, M. Reaume, N. Bultman, M. Patil, R. Quispe-Abad, J. Wei, Status and R&D of the target and beam dump at FRIB. in *8th High Power Targetry Workshop* (2023)

7 J.H. Holland, Genetic Algorithms. Sci. Am. **267**, 66–73 (1992)

8 S. Katoch, S.S. Chauhan, V. Kumar, A review on genetic algorithm: past, present, and future. Multimed. Tools Appl. **80**, 8091–8126 (2021). doi:10.1007/s11042-020-10139-6

9 J.C.S. Garcia et al., Multiobjective geometry optimization of microchannel heat exchanger using real-coded genetic algorithm. Appl. Therm. Eng. **202**, 117821 (2022). doi:10.1016/j.applthermaleng.2021.117821

10 T. Zhang, L. Chen, J. Wang, Multi-objective optimization of elliptical tube fin heat exchangers based on neural networks and genetic algorithm. Energy **269**, 126729 (2023). doi:10.1016/j.energy.2023.126729

11 F. Jin, D. Chen, L. Hu, Y. Huang, S. Bu, Optimization of zigzag parameters in printed circuit heat exchanger for supercritical CO2 Brayton cycle based on multi-objective genetic algorithm. Energy Convers. Manag. **270**, 116243 (2022). doi:10.1016/j.enconman.2022.116243

12 L. Meng, J. Liu, J. Bi, E.D. Özdemir, M.H. Aksel, Multi-objective optimization of plate heat exchanger for commercial electric vehicle based on genetic algorithm. Case Stud. Therm. Eng. **41**, 102629 (2023). doi:10.1016/j.csite.2022.102629

13 M.H. Hamed, A.N. Shmroukh, M. Attalla, H.M. Maghrabie, Optimization of inserted coiled tube three-fluid heat exchanger using genetic algorithms. Eng. Appl. Artif. Intell. **126**, 106909 (2023). doi:10.1016/j.engappai.2023.106909

14 B.S. Mekki, J. Langer, S. Lynch, Genetic algorithm based topology optimization of heat exchanger fins used in aerospace applications. Int. J. Heat Mass Transf. **170**, 121002 (2021). doi:10.1016/j.ijheatmasstransfer.2021.121002

15 A. Konak, D.W. Coit, A.E. Smith, Multi-objective optimization using genetic algorithms: A tutorial. Reliab. Eng. Syst. Saf. **91**, 992–1007 (2006). doi:10.1016/j.ress.2005.11.018

16 H. Keramati, F. Hamdullahpur, M. Barzegari, Deep reinforcement learning for heat exchanger shape optimization. Int. J. Heat Mass Transf. **194**, 123112 (2022). doi:10.1016/j.ijheatmasstransfer.2022.123112

17 Y.-Z. Wang, X.-J. He, Y. Hua, Z.-H. Chen, W.-T. Wu, Z.-F. Zhou, Closed-loop forced heat convection control using deep reinforcement learning. Int. J. Heat Mass Transf. **202**, 123655 (2023). doi:10.1016/j.ijheatmasstransfer.2022.123655

18 E. Ortiz-Mansilla, J.J. García-Esteban, J. Bravo-Abad, J.C. Cuevas, Deep reinforcement learning for radiative heat transfer optimization problems. Phys. Rev. Appl. **22**, 054071 (2024). doi:10.1103/physrevapplied.22.054071

19 E. Hachem, H. Ghraieb, J. Viquerat, A. Larcher, P. Meliga, Deep reinforcement learning for the control of conjugate heat transfer. J. Comput. Phys. **436**, 110317 (2021). doi:10.1016/j.jcp.2021.110317

20 X. Wang et al., Deep reinforcement learning-PID based supervisor control method for indirect-

contact heat transfer processes in energy systems. Eng. Appl. Artif. Intell. **117**, 105551 (2023). doi:10.1016/j.engappai.2022.105551
21 J. Li, Y. Li, T. Yu, Distributed deep reinforcement learning-based multi-objective integrated heat management method for water-cooling proton exchange membrane fuel cell. Case Stud. Therm. Eng. **27**, 101284 (2021). doi:10.1016/j.csite.2021.101284
22 G. Lee, Y. Joo, Y. Yu, H.-G. Kim, Dual-fluid topology optimization of printed-circuit heat exchanger with low-pumping-power design. Case Stud. Therm. Eng. **49**, 103318 (2023). doi:10.1016/j.csite.2023.103318
23 G. Lee, Y. Joo, S.-U. Lee, T. Kim, Y. Yu, H.-G. Kim, Design optimization of heat exchanger using deep reinforcement learning. Int. Commun. Heat Mass Transf. **159**, 107991 (2024). doi:10.1016/j.icheatmasstransfer.2024.107991
24 T. Haarnoja, A. Zhou, P. Abbeel, S. Levine, Soft Actor-Critic: Off-Policy Maximum Entropy Deep Reinforcement Learning with a Stochastic Actor. in *International Conference on Machine Learning*, pp. 1861–1870 (2018)
25 T. Haarnoja et al., Soft Actor-Critic Algorithms and Applications. arXiv:1812.05905 (2019). doi:10.48550/arXiv.1812.05905
26 P. D'Oro, M. Schwarzer, E. Nikishin, P.-L. Bacon, M.G. Bellemare, A. Courville, Sample-Efficient Reinforcement Learning by Breaking the Replay Ratio Barrier. in *NeurIPS 2022 Deep Reinforcement Learning Workshop* (2022)
27 G. Lee, J. Song, M. Patil, R. Quispe-Abad, N. Bultman, T. Kanemura, Design improvement of a minichannel beam dump wing through AI-driven Genetic Algorithms. in *16th International Conference on Heavy Ion Accelerator Technology (HIAT2025)* (2025). doi:10.18429/JACoW-HIAT2025-WEP11
28 G. Pintsuk et al., Interlaboratory Test on Thermophysical Properties of the ITER Grade Heat Sink Material Copper–Chromium–Zirconium. Int. J. Thermophys. **31**, 2147–2158 (2010). doi:10.1007/s10765-010-0857-y
29 Y.S. Touloukian, *Recommended Values of the Thermophysical Properties of Eight Alloys, Major Constituents and Their Oxides*. No. TEPIAC16. (1966)
30 S. Liu, S. Chang, H. Zhu, J. Yin, T. Wang, X. Zeng, Effect of substrate material on the molten pool characteristics in selective laser melting of thin wall parts. Int. J. Adv. Manuf. Technol. **105**, 3221–3231 (2019). doi:10.1007/s00170-019-04540-1
31 G. Syswerda, Uniform Crossover in Genetic Algorithms. in *International Conference on Genetic Algorithms*, pp. 2–9 (1989)
32 F. Herrera, M. Lozano, J.L. Verdegay, Tackling Real-Coded Genetic Algorithms: Operators and Tools for Behavioural Analysis. Artif. Intell. Rev. **12**, 265–319 (1998)
33 V. Mnih et al., Human-level control through deep reinforcement learning. Nature **518**, 529–533 (2015). doi:10.1038/nature14236
34 S. Fujimoto, H. Hoof, D. Meger, Addressing Function Approximation Error in Actor-Critic Methods. in *International Conference on Machine Learning*, pp. 1587–1596 (2018)
35 D.P. Kingma, J. Ba, Adam: A Method for Stochastic Optimization. arXiv:1412.6980 (2015). doi:10.48550/arXiv.1412.6980
36 J. Song et al., Design and experimental thermal validation of the mini-channel beam dump for FRIB. in *16th International Conference on Heavy Ion Accelerator Technology (HIAT2025)* (2025). doi:10.18429/JACoW-HIAT2025-TUP04